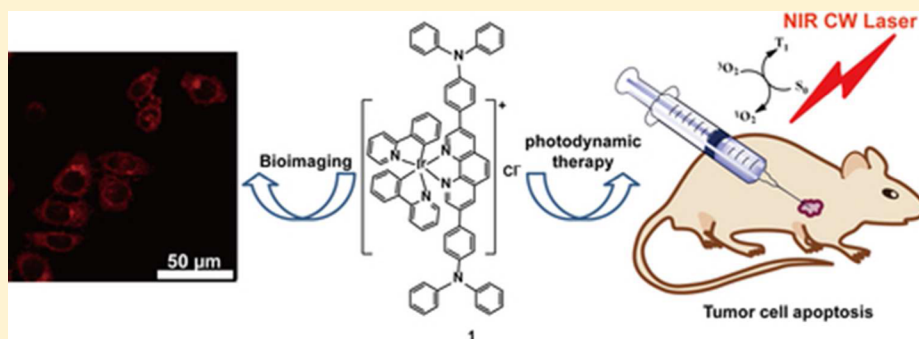


Two in One: Luminescence Imaging and 730 nm Continuous Wave Laser Driven Photodynamic Therapy of Iridium Complexes

Fengfeng Xue, Yang Lu, Zhiguo Zhou,* Min Shi, Yuping Yan, Hong Yang, and Shiping Yang*

The Key Laboratory of Resource Chemistry of Ministry of Education, Shanghai Key Laboratory of Rare Earth Functional Materials, and Shanghai Municipal Education Committee Key Laboratory of Molecular Imaging Probes and Sensors, Shanghai Normal University, No. 100, Guilin Road, Shanghai 200234, People's Republic of China

Supporting Information



ABSTRACT: A phosphorescent cationic iridium complex (**1**) with a donor– π -donor type unit as a N^N ligand and 2-phenylpyridine as a C^N ligand was synthesized and characterized. **1** exhibits an intense absorption peak centered at ~ 450 nm with a large molar extinction coefficient (ϵ) of $\sim 2.4 \times 10^4$ M⁻¹ cm⁻¹ and displays highly efficient orange-red phosphorescence located at 620 nm with a quantum efficiency of $\sim 3\%$ in PBS buffer solution at room temperature, which is beneficial for a luminescence probe in living cells excited by visible light. Importantly, the generation of singlet oxygen ($^1\text{O}_2$) by **1** was observed by 730 nm continuous wave (CW) laser irradiation owing to its reverse saturable absorption property, which was confirmed by the $^1\text{O}_2$ scavenger of 1,3-diphenylbenzo[*c*]furan (DPBF) and ESR spectra. The photodynamic therapy effect of **1** in vivo by a 730 nm CW laser was further assessed by histological examination and immunohistochemistry.

1. INTRODUCTION

Cyclometalated iridium complexes have been playing a vital role in bioimaging^{1–6} due to their metal-to-ligand charge transfer transition (MLCT), which displayed the excellent photophysical properties of a large Stokes shift, variable absorption/emission wavelength, and high quantum efficiency. In particular, the heavy atom iridium in the complexes can induce strong spin–orbit coupling to enhance efficient singlet–triplet intersystem crossing for the generation of singlet oxygen ($^1\text{O}_2$), and the application of these complexes has also been extended into the field of photodynamic therapy.^{7–11} The phosphorescence property and the $^1\text{O}_2$ generation ability of iridium complexes provide unique advantages for their application in the field of theranostics. To date, few iridium complexes have been reported as theranostic agents. For example, Lo's group⁷ reported a series of phosphorescent cyclometalated iridium polypyridine poly(ethylene glycol) (PEG) complexes for mitochondria-targeting luminescent imaging and photodynamic therapy upon 365 nm UV-lamp irradiation. To extend the light irradiation to the visible region, Aoki's group⁹ reported a pH-sensitive cyclometalated iridium(III) complex for luminescence imaging of the acidic intracellular organelles and PDT upon photoirradiation of

470 nm. Chou's group^{10,11} developed iridium complex functionalized nanoparticles, including Fe₃O₄/SiO₂ core/shell nanoparticles and CdSe/ZnS quantum dots, for theranostic applications. Unfortunately, the absorption band of conventional Ir(III) complexes is mainly located in the UV to visible light region.¹² Due to the smaller penetration depth of UV and visible light, the application of Ir(III) complexes in PDT in vivo has not reported. Considering that near-infrared (NIR) light (700–1100 nm) exhibits low attenuation by blood and soft tissues, NIR light triggered PDT can effectively overcome the above disadvantages.^{13–18} Therefore, it is necessary to develop Ir(III) complexes with NIR absorption for PDT in vivo. Recently, the Zhao group reported cyclometalated iridium(III) complexes containing monostyryl/distyryl BODIPY ligands with strong near-infrared (NIR) absorption and phosphorescence as a theranostic agent for luminescence imaging and PDT in vitro by a 635 nm LED.¹⁹ Herein, we incorporate an iridium center into a donor– π -donor type ligand to obtain the cationic Ir(III) complex **1**. Due to the phosphorescence property and low cytotoxicity, **1** could be used for luminescent

Received: August 31, 2014

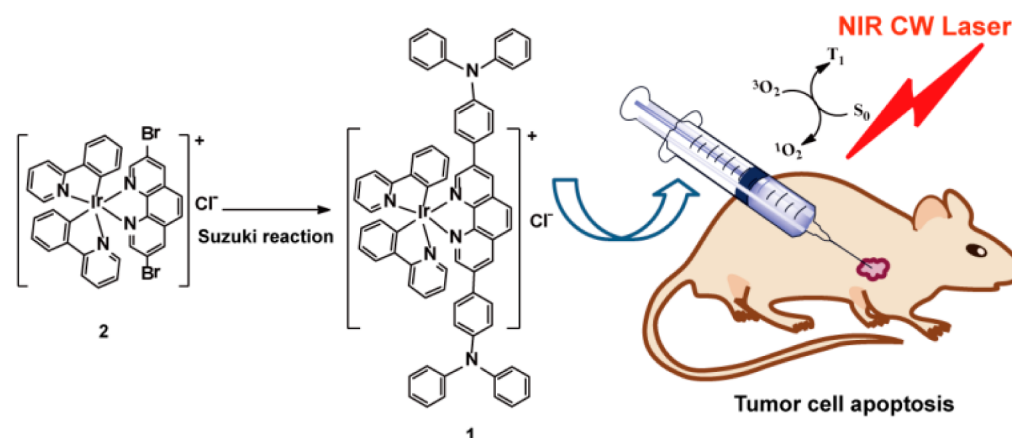


Figure 1. Schematic illustration of 730 nm CW laser driven PDT on the xenograft HeLa tumor model.

imaging in living cells. Furthermore, by use of its reverse saturable absorption, singlet oxygen ($^1\text{O}_2$) has been effectively generated on irradiation by a 730 nm continuous wave (CW) laser. As a proof of concept, 730 nm CW laser driven PDT of **1** in vivo has been further confirmed on the xenograft HeLa tumor model by histological examination and immunohistochemistry (Figure 1).

2. EXPERIMENTAL SECTION

2.1. Materials and Characterization. $\text{IrCl}_3 \cdot \text{H}_2\text{O}$ and 2-phenylpyridine (ppy) were purchased from Shanghai Jiuyue Chemical Co. and Shanghai Ruiyi Medical Tech. Co. Ltd., respectively. Other chemical reagents were bought from Sinopharm Chemical Reagent Co. Ltd. All solvents were dried by a conventional procedure prior to use. 3,8-Dibromophenanthroline²⁰ and cyclometalated iridium chloro-bridged dimer²¹ were synthesized according to the literature.

^1H NMR and ^{13}C NMR spectra were measured on a Bruker DMX400 NMR spectrometer at room temperature. Mass spectra were measured on a MALDI-TOF instrument (Shimadzu, Japan). The photoluminescence and absorption spectra were measured on a fluorescence spectrophotometer (Varian) and absorption spectrophotometer (UV-7502PC), respectively. Luminescence lifetimes were determined with an Edinburgh spectrophotometer (FL 920) excited by a 375 nm laser. ESR spectra were recorded on a Bruker EMX-8/2.7 spectrometer at 9.872 GHz (X-band with 100 kHz field modulation).

2.2. Synthesis of Iridium Complex 1. A mixture of $[(\text{ppy})_2\text{Ir}(\mu\text{-Cl})_2\text{Ir}(\text{ppy})_2]$ (0.25 mmol, 267.9 mg) and 3,8-dibromophenanthroline (0.60 mmol, 202.8 mg) was added to the mixed solution of CH_2Cl_2 and CH_3OH (2/1 v/v). After the solution was refluxed for 6 h, the solvent was removed by vacuum distillation. The crude product was separated by a chromatographic column using $\text{CH}_2\text{Cl}_2/\text{CH}_3\text{OH}$ (50/1 v/v) as an eluent to afford a red solid in a yield of 90%. ^1H NMR (400 MHz, $\text{DMSO}-d_6$): δ (ppm) 9.19 (d, 2H, $J = 2.0$ Hz), 8.67 (s, 2H), 8.16 (d, 2H, $J = 2.0$ Hz), 7.96 (d, 2H, $J = 8.0$ Hz), 7.79 (t, 2H, $J = 7.8$ Hz), 7.73 (d, 2H, $J = 7.2$ Hz), 7.35 (d, 2H, $J = 5.6$ Hz), 7.09 (t, 2H, $J = 7.2$ Hz), 6.99 (q, 4H, $J = 6.4$ Hz), 6.34 (d, 2H, $J = 7.2$ Hz). ^{13}C NMR (100 MHz, $\text{DMSO}-d_6$): δ 166.99, 151.83, 151.38, 150.72, 148.95, 145.11, 144.82, 144.18, 141.52, 139.62, 138.56, 132.77, 131.94, 130.96, 130.47, 129.37, 127.94, 125.83, 124.74, 123.44, 122.62, 120.75, 120.32. MS (MALDI-TOF): calcd for $\text{IrC}_{34}\text{H}_{24}\text{N}_4\text{Br}_2^+$ 839.0 (M^+), found 839.1 (M^+).

4-(*S,S*-Dimethyl-1,3,2-dioxaborinan-2-yl)-*N,N*-diphenylaniline (0.33 mmol, 118.9 mg) was mixed with **2** (0.80 mmol, 285.7 mg) in DMF (40 mL) under a nitrogen atmosphere. A 10 mL portion of a 2 M K_2CO_3 solution in water and $\text{Pd}(\text{PPh}_3)_4$ (5 mol %) were added, and then this mixture was refluxed for 24 h. After the temperature decreased to room temperature, deionized water (200 mL) was added. The mixture was extracted with CH_2Cl_2 . After the extract was dried over MgSO_4 , the organic solvent was removed by vacuum distillation.

The obtained product was purified by a chromatographic column using $\text{CH}_2\text{Cl}_2/\text{CH}_3\text{OH}$ (50/1 v/v) as eluent to afford the red solid **1** in a yield of 75%. ^1H NMR (400 MHz, $\text{DMSO}-d_6$): δ 9.03 (s, 1H), 8.58 (s, 1H), 8.41 (s, 1H), 8.04 (s, 1H), 7.94 (d, $J = 8.2$ Hz, 1H), 7.76 (t, $J = 9.5$ Hz, 2H), 7.46 (t, $J = 8.4$ Hz, 1H), 7.41 (d, $J = 8.3$ Hz, 2H), 7.31 (t, $J = 6.7$ Hz, 3H), 7.29 (d, $J = 5.4$ Hz, 2H), 7.12 (dd, $J = 11.6$, 8.7 Hz, 8H), 6.98 (t, $J = 7.1$ Hz, 2H), 6.46 (d, $J = 7.5$ Hz, 1H). ^{13}C NMR (100 MHz, $\text{DMSO}-d_6$): δ 168.03, 162.77, 149.91, 149.63, 148.79, 148.59, 147.06, 145.01, 143.95, 138.52, 134.48, 132.15, 131.73, 131.09, 129.78, 128.14, 127.42, 125.60, 125.02, 124.30, 123.71, 123.11, 122.71, 119.95. HRMS (ESI⁺): calcd for $\text{IrC}_{70}\text{H}_{50}\text{N}_6^+$ 1167.3726 (M^+), found 1167.3715 (M^+).

2.3. Generation of $^1\text{O}_2$ of **1 in Solution.** For the method of absorption spectroscopy, a solution of **1** (3 mL) in an ethanol/water (4/1 v/v) solution (1.0×10^{-5} M) and DPBF (5.0×10^{-5} M) was illuminated by a 730 nm CW laser ($0.5 \text{ W}/\text{cm}^2$) every 1 min to observe the decrease of the absorbance of DPBF centered at 410 nm.

For the method of electron spin resonance spectroscopy (ESR), a solution of **1** (3 mL) in an ethanol/water (4/1 v/v) solution (1.0×10^{-5} M) and 2,2,6,6-tetramethyl-4-piperidone (TEMP; 5.0×10^{-5} M) was illuminated by a 730 nm CW laser ($0.5 \text{ W}/\text{cm}^2$) for 10 min to observe the ESR signal of radical nitroxides.

2.4. Confocal Luminescence Imaging. After HeLa cells (5×10^8 /L) were incubated with **1** ($20 \mu\text{M}$) for 30 min at 37°C , they were washed three times with PBS. Luminescence imaging was measured on a laser confocal scanning microscope (Leica DMI 6000B) with a 63 \times objective lens excited by a 405 nm laser. The emission was collected at 620 ± 30 nm.

2.5. Flow Cytometry. To determine the uptake content of **1**, HeLa cells were incubated with **1** ($20 \mu\text{M}$) in serum-free medium for 2 h. After the cells were rinsed three times with PBS, the cells were harvested by trypsinization and then determined by flow cytometry. The data were analyzed with WinMDI 2.9.

2.6. In Vivo Photodynamic Therapy on a HeLa Xenograft Tumor Model. HeLa cells were incubated to the nude mice ($n = 4-6$ weeks old). When the tumor length reached 20–30 mm, the mice were intratumorally injected with **1** (30 mg kg^{-1} body weight on dissolution in saline/DMSO 49/1) and then irradiated by a 730 nm CW laser ($0.2 \text{ W}/\text{cm}^2$) for 10 min every 2 days. Control groups were as follows: control group 1, mice injected with the saline solution ($200 \mu\text{L}$); control group 2, mice injected with **1** with the same dose; control group 3, mice irradiated by a 730 nm CW laser ($0.2 \text{ W}/\text{cm}^2$) for 10 min every 2 days. After treatment for 14 days, the tumors were taken out, fixed with 4% paraformaldehyde, and embedded in paraffin for H&E, TUNEL, and HO-1 staining according to the standard procedure.

3. RESULTS AND DISCUSSION

3.1. Synthesis and Photophysical Properties of **1.** Iridium complex **2** was synthesized according to the general

method of the cyclometalated iridium complex.²² The triphenylamine unit as a strong electron donor was conjugated to **2** by a Suzuki reaction to form **1**. The absorption spectrum of **1** in DMSO/PBS (1/49 v/v) is presented in Figure 2. The

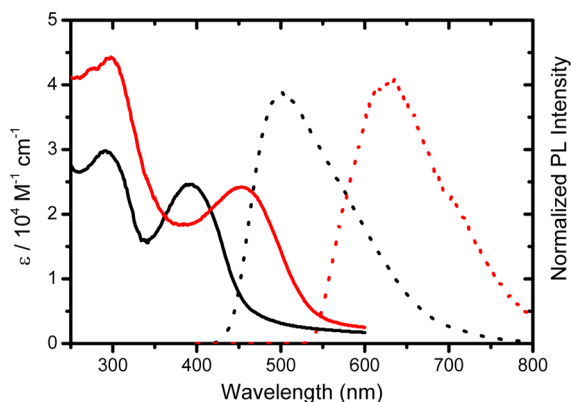


Figure 2. Absorption spectra of the N^N ligand (black solid line) and **1** (red solid line) and phosphorescence spectra of the N^N ligand (black dashed line) and **1** (red dashed line) in DMSO/PBS (1/49 v/v) solution.

strong absorption band around 300 nm is attributed to an intraligand $\pi-\pi^*$ transition. An intense absorption band centered at ~ 450 nm had a molar extinction coefficient (ϵ) of $2.4 \times 10^4 \text{ M}^{-1} \text{ cm}^{-1}$. In comparison to the complex Ir(ppy)₂(phen) (ppy = 2-phenylpyridine, phen = 1,10-phenanthroline), in which the visible absorption is due to the ³MLCT transition,²¹ the large absorption coefficient indicated that the visible absorption should be attributed to an intraligand $\pi-\pi^*$ transition.²³ The >60 nm red shift of **1** in comparison to that of the ligand was due to the cationic property of the

iridium center on the N^N ligand (Figure S1, Supporting Information). The room-temperature photoluminescence spectra in DMSO/PBS (1/49 v/v) showed that iridium complex **1** exhibited a red intense emission located at 620 nm resulting from the competition between ³MLCT and ³IL, which gives long-lived emission; the long lifetime is $\sim 1.3 \mu\text{s}$.²³ The quantum efficiency was above 3% in the PBS buffer solution using an aerated [Ru(bpy)₃]Cl₂ solution ($\phi = 0.028$) as the standard solution,²⁴ which can be an advantage for the luminescence imaging.

3.2. Luminescence Imaging of 1. For biological applications, biocompatibility is one of the most important problems to be addressed. Therefore, the cytotoxicity of **1** was first investigated by the standard MTT assay using HeLa cells as a model cancer cell line. As shown in Figure 3a, no obvious change in the cell viability of HeLa cells could be observed after incubation with different concentrations of **1**. The viability was calculated to be greater than $\sim 85\%$ at a concentration of $50 \mu\text{M}$, indicating that it should be a promising candidate as a luminescent probe in living cells. The endocytosis of **1** by HeLa cells was evaluated by flow cytometry. As shown in Figure 3b, more than 90% of the HeLa cells incubated with a concentration of $20 \mu\text{M}$ for 2 h were marked, suggesting effective uptake of **1** by living cells. Promoted by the effective internalization of **1**, luminescence imaging was performed. HeLa cells were incubated with **1** ($20 \mu\text{M}$) for 2 h, and then the intense luminescence in cells was observed on 405 nm excitation (Figure 3c). The overlay of bright field and luminescence images confirmed that **1** should be mainly located inside the cytoplasm without obvious nuclear uptake. These data supported that **1** could be developed as a luminescent biomarker.

3.3. Generation of ¹O₂ and Photodynamic Therapy Driven by NIR Laser. Considering the heavy-atom effect of

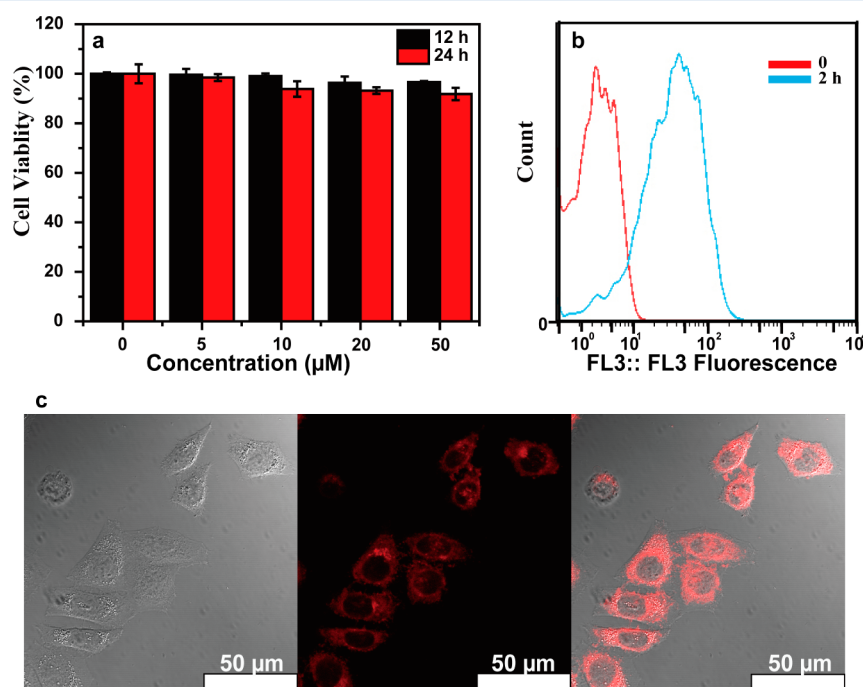


Figure 3. (a) Cell viability of HeLa cells assessed using an MTT assay after the incubation of different concentrations of **1** for 12 and 24 h, respectively. (b) Flow cytometry analysis of HeLa cells incubated with **1** ($20 \mu\text{M}$) for 2 h. (c) Bright field (left), confocal luminescence (middle), and overlay (right) images of HeLa cells incubated with **1** ($20 \mu\text{M}$) for 2 h.

the iridium center, we investigated the generation of $^1\text{O}_2$. To our surprise, the generation of $^1\text{O}_2$ was observed on irradiation by a 730 nm CW laser. As is known, 1,3-diphenylbenzo[*c*]furan (DPBF) is usually used as an efficient $^1\text{O}_2$ scavenger to produce its oxidized product of 1,2-dibenzoylbenzene.²⁵ The absorption centered at 410 nm decreased 90% after irradiation by a 730 nm CW laser for 10 min (0.5 W/cm^2) in the presence of **1** (Figure 4a). $\ln(A_t/A_0)$ values exhibited a good linear relation-

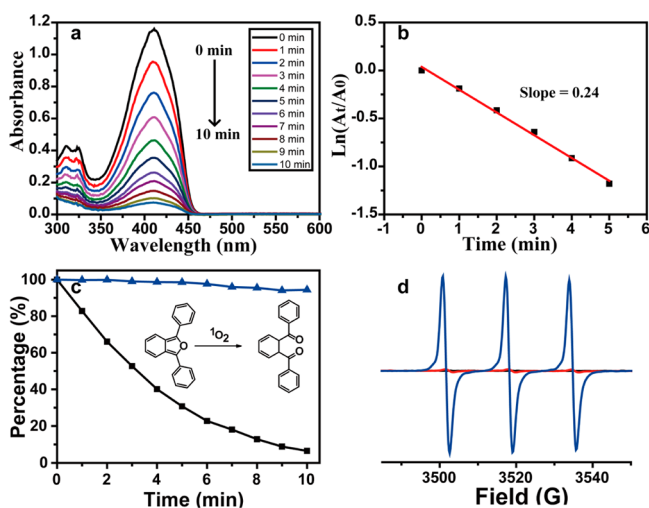


Figure 4. (a) Changes in the absorption spectra of a DPBF solution in the presence of **1** in air-saturated ethanol/water (4/1 v/v) solution irradiated by a 730 nm CW laser. (b) Comparative plots of $\ln(A_t/A_0)$ as a function of time. A_0 is the initial absorbance, and A_t is the absorbance at different irradiation times. (c) Decay profiles of the absorbance of DPBF centered at 410 nm in the presence of **1** (black) and **1** with NaN_3 ($5.0 \times 10^{-5} \text{ M}$; blue) in air-saturated ethanol/water (4/1 v/v) solution irradiated by a 730 nm CW laser. The inset gives the reaction mechanism for $^1\text{O}_2$ detection with DPBF. (d) ESR signals of a TEMP solution irradiated by a 730 nm CW laser (black), TEMP and **1** (red), and TEMP and **1** irradiated by a 730 nm CW laser (blue) of an air-saturated ethanol/water (4/1 v/v) solution. The concentration of TEMP was $5 \times 10^{-5} \text{ M}$. The concentration of **1** was $1.0 \times 10^{-5} \text{ M}$. The power density of the 730 nm CW laser was 0.5 W/cm^2 .

ship with the irradiation time. The photo-oxidation rate expressed by the slope of the linear plot was calculated to be 0.24 min^{-1} (Figure 4b). The photochemical stability of **1** was also investigated by monitoring the changes in UV-vis absorption spectra with the continuous irradiation of a 730 nm CW laser. Little change was observed with 10 min of continuous irradiation (Figure S7, Supporting Information), suggesting its satisfactory photostability to a 730 nm CW laser. To further confirm the generation of $^1\text{O}_2$, an inhibition experiment was carried out. In the presence of NaN_3 , a quencher of $^1\text{O}_2$, no obvious change in the absorption of DPBF was observed (Figure 4c). On the basis of the reaction of $^1\text{O}_2$ with 2,2,6,6-tetramethyl-4-piperdione (TEMP) to form the stable free radical nitroxides,²⁶ an obvious ESR signal of radical nitroxides was observed in the presence of **1** irradiated by a 730 nm CW laser (Figure 4d). However, no ESR was found in a solution of TEMP only irradiated by a 730 nm CW laser or a solution of **1** and TEMP. All of these experimental results suggested that $^1\text{O}_2$ was generated by a 730 nm CW laser. To explore the mechanism for 730 nm driven PDT, the nonlinear absorption of **1** in ethanol/water solution was determined on a 4f coherent imaging system according to the literature.²⁷ As

expected, **1** showed nonlinear absorption on excitation by a 730 nm nanosecond laser. An image was recorded with a CCD camera. The nonlinear image and the fitting curve for the experimental data are shown in Figure S8 in the Supporting Information. The nonlinear absorption coefficient (β) was calculated to be $-2.7 \times 10^{-12} \text{ m/W}$, which indicated that the nonlinear absorption of **1** could be attributed to the reverse saturable absorption. Therefore, the reverse saturable absorption should be responsible for the 730 nm laser driving the generation of $^1\text{O}_2$.

Encouraged by the efficient generation of $^1\text{O}_2$ of **1** driven by a 730 nm CW laser, photodynamic therapy in vivo was assessed by histological examination and immunohistochemistry. HeLa tumor bearing mice were intratumorally injected with complex **1** (30 mg/kg body weight) and then irradiated by a 730 nm CW laser (0.2 W/cm^2) for 10 min every 2 days. For the control experiments, HeLa tumor bearing mice were only intratumorally injected with the same dose of **1** or irradiated by a 730 nm CW laser alone. After 14 days, H&E staining was used to examine the damage levels of tumor tissues. The experimental group showed a higher damage level of the tumor tissue in comparison with those treated with only **1** or 730 nm CW laser irradiation alone (Figure 5a), suggesting that

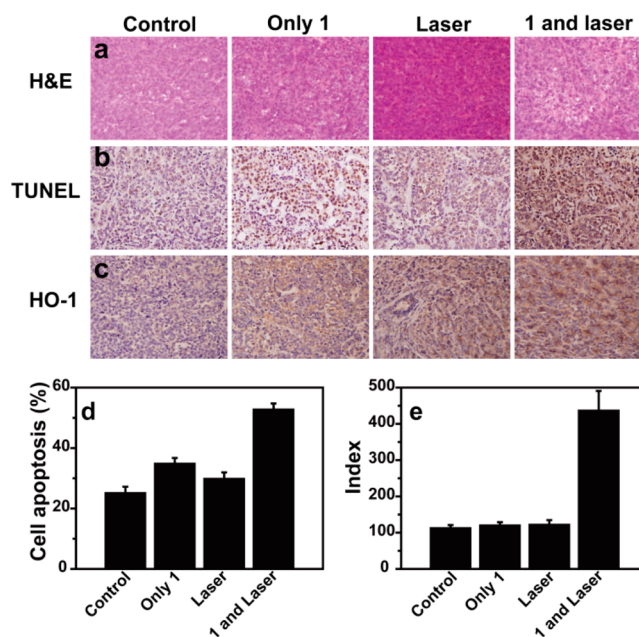


Figure 5. (a–c) H&E (a), TUNEL (b), and HO-1 (c) staining images of representative specimens at 400 \times magnification after PDT for 14 days. (d) TUNEL positive percentage of tumor tissues determined by a TUNEL assay. (e) HO-1 positive percentage of tumor tissues determined by an HO-1 assay. Index denotes the immunohistochemical index.

1 could kill tumor cells effectively by treatment with a 730 nm CW laser. To quantitatively illustrate the extent of the damage to tumor tissues, TUNEL staining was performed. The tumor tissue in the experimental group had extensive regions of apoptotic cells stained in brown (Figure 5b). On the basis of the experimental results, $52.7 \pm 2.0\%$ TUNEL positive cells were found in the experimental group. However, only $25.1 \pm 2.4\%$, $34.0 \pm 1.8\%$, and $29.7 \pm 2.2\%$ TUNEL positive cells were observed for the control group only injected intratumorally with the saline solution, injected with **1**, and irradiated by a 730

nm CW laser alone, respectively. According to the experimental data, the percentages of the TUNEL positive cells resulting from **1** and the laser were ~8.9% (the difference between the TUNEL positive cells resulting from **1** and the control group) and ~4.6% (the difference between the TUNEL positive cells resulting from the laser and control groups), respectively. However, the coeffect value was ~27.6% (the difference between the TUNEL positive cells resulting from the experimental and control groups), which was much higher than the sum of the two individual effects (~13.5%). This fact confirmed the PDT effect of **1** irradiated by a 730 CW laser. To further confirm the apoptotic mechanism of tumor cells, heme oxygenase (HO-1) staining was performed. The expression of HO-1 greatly increases by stressful conditions such as oxidative stress, hypoxia, heavy-metal ions and so on, and the major role of this enzyme is protection against photodynamic therapy.²⁸ As shown in Figure 5e, more than 4 times greater expression of HO-1 in tumors of the experimental group was found in comparison with that of the control group only injected intratumorally with **1** or irradiated by a 730 nm CW laser alone, which directly demonstrated that **1** can act as a photodynamic agent for 730 nm CW laser driven photodynamic therapy. To our regret, there is no apparent change in tumor size after the treatment by a 730 nm CW laser for 2 weeks. Therefore, to perform good PDT in vivo, it is necessary to design an iridium complex with a larger nonlinear absorption coefficient.

4. CONCLUSIONS

In summary, we have successfully synthesized a new phosphorescent iridium complex with a D- π -D conjugated ligand. The photophysical properties indicate that **1** can act as a bioprobe for luminescence imaging in living cells. More importantly, singlet oxygen was generated on irradiation by a 730 nm CW laser. Photodynamic therapy on the xenograft HeLa tumor model demonstrated that ¹O₂ can cause the apoptosis of tumor cells. This is a powerful example of photodynamic therapy by NIR nonlinear techniques. However, the PDT effect of the iridium complex in vivo was not good enough. There is still a long way to go in exploring iridium complexes with a larger nonlinear absorption coefficient for the practical application of PDT in vivo.

■ ASSOCIATED CONTENT

Supporting Information

Figures giving ¹H NMR and ¹³C NMR spectra, a mass spectrum, photostability of **1**, and nonlinear image of **1** on a 4f coherent imaging system. This material is available free of charge via the Internet at <http://pubs.acs.org>.

■ AUTHOR INFORMATION

Corresponding Authors

*E-mail for Z.Z.: zgzhou@shnu.edu.cn;

*E-mail for S.Y.: shpingy@shnu.edu.cn.

Notes

The authors declare no competing financial interest.

■ ACKNOWLEDGMENTS

This work was partially supported by the National Natural Science Foundation of China (Nos. 21271130 and 21371122), the Program for Changjiang Scholars and Innovative Research Team in University (No. IRT1269), the Shanghai Science and Technology Fund Program (Nos. 12ZR1421800 and

13520502800), the Shanghai Pujiang Program (13PJ1406600), the Shanghai Municipal Education Commission (Nos. 13ZZ110 and 14YZ073), Shanghai Normal University (No. SK201339), and the International Joint Laboratory on Resource Chemistry (IJLRC).

■ REFERENCES

- (1) Yu, M.; Zhao, Q.; Shi, L.; Li, F.; Zhou, Z.; Yang, H.; Yi, T.; Huang, C. *Chem. Commun.* **2008**, 2115–2117.
- (2) Lo, K. K.-W.; Louie, M.-W.; Zhang, K. Y. *Coord. Chem. Rev.* **2010**, *254*, 2603–2622.
- (3) Lo, K. K.-W.; Zhang, K. Y. *RSC Adv.* **2012**, *2*, 12069–12083.
- (4) Li, C.; Yu, M.; Sun, Y.; Wu, Y.; Huang, C.; Li, F. *J. Am. Chem. Soc.* **2011**, *133*, 11231–11239.
- (5) Liu, Q.; Yin, B.; Yang, T.; Yang, Y.; Shen, Z.; Yao, P.; Li, F. *J. Am. Chem. Soc.* **2013**, *135*, 5029–5037.
- (6) Liu, Q.; Yang, T.; Feng, W.; Li, F. *J. Am. Chem. Soc.* **2012**, *134*, 5390–5397.
- (7) Li, S. P.-Y.; Lau, C. T.-S.; Louie, M.-W.; Lam, Y.-W.; Cheng, S. H.; Lo, K. K.-W. *Biomaterials* **2013**, *34*, 7519–7532.
- (8) Peng, Y.-K.; Lai, C.-W.; Liu, C.-L.; Chen, H.-C.; Hsiao, Y.-H.; Liu, W.-L.; Tang, K.-C.; Chi, Y.; Hsiao, J.-K.; Lim, K.-E.; Liao, H.-E.; Shyue, J.-J.; Chou, P.-T. *ACS Nano* **2011**, *5*, 4177–4187.
- (9) Moromizato, S.; Hisamatsu, Y.; Suzuki, T.; Matsuo, Y.; Abe, R.; Aoki, S. *Inorg. Chem.* **2012**, *51*, 12697–12706.
- (10) Lai, C.-W.; Wang, Y.-H.; Lai, C.-H.; Yang, M.-J.; Chen, C.-Y.; Chou, P.-T.; Chan, C.-S.; Chi, Y.; Chen, Y.-C.; Hsiao, J.-K. *Small* **2008**, *4*, 218–224.
- (11) Hsieh, J.-M.; Ho, M.-L.; Wu, P.-W.; Chou, P.-T.; Tsai, T.-T.; Chi, Y. *Chem. Commun.* **2006**, 615–617.
- (12) Stacey, O. J.; Pope, S. J. A. *RSC Adv.* **2013**, *3*, 25550–25564.
- (13) Zhang, M.; Murakami, T.; Ajima, K.; Tsuchida, K.; Sandanayaka, A. S. D.; Ito, O.; Iijima, S.; Yudasaka, M. *Proc. Natl. Acad. Sci. USA* **2008**, *105*, 14773–14778.
- (14) Zhang, P.; Steelant, W.; Kumar, M.; Scholfield, M. *J. Am. Chem. Soc.* **2007**, *129*, 4526–4527.
- (15) Gao, D.; Agayan, R. R.; Xu, H.; Philbert, M. A.; Kopelman, R. *Nano Lett.* **2006**, *6*, 2383–2386.
- (16) Gorman, A.; Killoran, J.; O'Shea, C.; Kenna, T.; Gallagher, W. M.; O'Shea, D. F. *J. Am. Chem. Soc.* **2004**, *126*, 10619–10631.
- (17) Kalluru, P.; Vankayala, R.; Chiang, C.-S.; Hwang, K. C. *Angew. Chem., Int. Ed.* **2013**, *52*, 12332–12336.
- (18) Idris, N. M.; Gnanasammandhan, M. K.; Zhang, J.; Ho, P. C.; Mahendran, R.; Zhang, Y. *Nat. Med.* **2012**, *18*, 1580–1585.
- (19) Sun, H.; Yang, L.; Yang, H.; Liu, S.; Xu, W.; Liu, X.; Tu, Z.; Su, H.; Zhao, Q.; Huang, W. *RSC Adv.* **2013**, *3*, 8766–8776.
- (20) Li, W.-J.; Wu, H.-M.; Li, Y.-B.; Hu, C.-P.; Yi, M.-D.; Xie, L.-H.; Chen, L.; Zhao, J.-F.; Zhao, X.-H.; Shi, N.-E.; Qian, Y.; Wang, C.; Wei, W.; Huang, W. *Tetrahedron* **2012**, *68*, 8216–8221.
- (21) Xue, F.; Lu, Y.; Zhou, Z.; Zhang, C.; Fang, S.; Yang, H.; Yang, S. *J. Coord. Chem.* **2014**, 1–14.
- (22) Qin, L.; Zhu, Y.; Yang, H.; Ding, L.; Sun, F.; Shi, M.; Yang, S. *Mater. Chem. Phys.* **2013**, *139*, 345–349.
- (23) Lincoln, R.; Kohler, L.; Monroe, S.; Yin, H.; Stephenson, M.; Zong, R.; Chouai, A.; Dorsey, C.; Hennigar, R.; Thummel, R. P.; McFarland, S. A. *J. Am. Chem. Soc.* **2013**, *135*, 17161–17175.
- (24) Nakamaru, K. *Bull. Chem. Soc. Jpn.* **1982**, *55*, 2697–2705.
- (25) Zhou, Q.-X.; Lei, W.-H.; Chen, J.-R.; Li, C.; Hou, Y.-J.; Wang, X.-S.; Zhang, B.-W. *Chem. Eur. J.* **2010**, *16*, 3157–3165.
- (26) Ding, H.-Y.; Wang, X.-S.; Song, L.-Q.; Chen, J.-R.; Yu, J.-H.; Chao, L.; Zhang, B.-W. *J. Photochem. Photobiol. A* **2006**, *177*, 286–294.
- (27) Li, Y.; Yang, K.; Zhang, X.; Chang, Q.; Wang, Y.; Song, Y. *Opt. Commun.* **2008**, *281*, 3913–3918.
- (28) Nowis, D.; Legat, M.; Grzela, T.; Niderla, J.; Wilczek, E.; Wilczynski, G. M.; Glodkowska, E.; Mrowka, P.; Issat, T.; Dulak, J.; Jozkowicz, A.; Was, H.; Adamek, M.; Wrzosek, A.; Nazarewski, S.; Makowski, M.; Stoklosa, T.; Jakobisiak, M.; Golab, J. *Oncogene* **2006**, *25*, 3365–3374.